ISSN 1070-3632, Russian Journal of General Chemistry, 2010, Vol. 80, No. 6, pp. 1128–1135. © Pleiades Publishing, Ltd., 2010.
Original Russian Text © E.P. Domashevskaya, V.A. Terekhov, S.Yu. Turishchev, D.A. Khoviv, E.V. Parinova, V.A. Skryshevskii, I.V. Garil'chenko, 2010, published in Zhurnal Obshchei Khimii, 2010, Vol. 80, No. 6, pp. 958–965.

Atomic and Electronic Structure of the Surface of Porous Silicon Layers

E. P. Domashevskaya[a], V. A. Terekhov[a], S. Yu. Turishchev[a], D. A. Khoviv[a], E. V. Parinova[a], V. A. Skryshevskii[b], and I. V. Garil'chenko[b]

[a] *Voronezh State University, Universitetskaya pl. 1, Voronezh, 394006 Russia*
e-mail: ftt@phys.vsu.ru

[b] *Shevchenko Kiev National University, Kiev, Ukraine*

Received January 13, 2010

Abstract—Atomic and electronic structure of the surface layers of porous silicon was studied by the methods of the near fine structure spectroscopy at the edge of X-ray absorption and ultrasoft X-ray emission spectroscopy. The thickness of the oxide layer and the degree of distortion of silicon–oxygen tetrahedra in this layer were estimated. The thickness of the surface oxide layer on the amorphous layer covering the nanocrystals of porous silicon that was kept during one year is several times greater than the thickness of the natural oxide in the single crystal silicon wafers. Distortion of the silicon–oxygen tetrahedron, the basic structural units of the silicon oxide, is accompanied by elongation of Si–O bonds and an increase in the Si–O–Si bond angles.

DOI: 10.1134/S1070363210060150

Producing of silicon nanocrystals for creation of effective photoluminescent structures based on silicon technology is performed in different ways. One is an electrochemical method of producing porous silicon. A numerous studies have shown convincingly that porous silicon is one of the most promising materials for nano- and optoelectronics. In a handbook on the IR spectroscopy of ultrathin films a significance of the effect of Si–H hydrogen bonds on the photoluminescence of porous silicon was indicated [1]. Our studies of porous silicon by the method of ultrasoft X-ray spectroscopy showed that the porous silicon consists of the silicon nanocrystals coated with an amorphous layer of elemental silicon, most likely, hydrogenated, that is, a-Si:H, and oxide nanolayers, which include suboxide [2, 3]. We have shown that the quantitative ratio of the porous silicon phases depends essentially on the type of substrate and changes in time at exposure to the atmosphere [4].

To date a number of models is known describing visible photoluminescence in porous silicon: quantum-size effect [5, 6], surface passivation [7], the photoluminescence due to the presence of the interface Si–SiO_2 [8, 9], etc. However, none of them can explain all known experimental data, including the data concerning the processes of changes in the photoluminescence properties in time. It should be noted that the problem of stability and degradation of the photoluminescence properties associated with the phase composition and electron energy structure remains urgent. In [3, 10] we have presented a model of photoluminescence in porous silicon on the basis of the data obtained by ultrasoft X-ray spectroscopy, as a result of the zone–zone electron transitions between energy levels of nano-crystalline, amorphous and oxide phases covering the silicon nanocrystals. All the results presented in the above listed publications were obtained on the silicon of *n*-type doped with phosphorus and antimony.

The aim of this work is to study the characteristics of the atomic and electronic structure of surface oxide and amorphous layers covering the nanocrystals of porous silicon, obtained on the single-crystal silicon wafers of *p*-type silicon doped with boron (BDSi).

The samples of porous silicon were formed by electrochemical anodic etching of single crystal wafers Si(100) doped with boron (BDSi) with a specific resistance 4.5 Ω cm. The porous-Si samples obtained at three different durations of anodic etching: 0.5, 2.0, 3.0 min, are designated as porous silicon (0.5), porous

silicon (2.0) and porous silicon (3.0), respectively. Sample of porous silicon (0.5) was etched at a current density of 5 mA cm^{-2}, whereas the remaining samples at a current density of 20 mA cm^{-2}. At the initial stage of etching the etching rate was about 5–10 nm s^{-1}, and then it slowed.

The study by the method of fine structure spectroscopy, near edge X-ray absorption XANES (X-ray absorption near edge structure) near the $L_{2,3}$-edge of silicon absorption were carried out at the SRC synchrotron of the University of Wisconsin–Madison (Stoughton, USA). The vacuum in the chamber was 10^{-10} Torr, hardware broadening 0.05 eV, the depth of analysis about 5 nm. The XANES spectra were recorded by measuring the current from the sample. In the ultrasoft region of the XANES spectrum, due to a very high extinction coefficient not the extinction at the passing of synchrotron radiation through an object is registered as in "hard" X-ray or optical region [11], but the quantum yield of the electrons of external X-ray photoeffect in the region of the extinction edge [12]. Therefore the multiplier registers directly photo- and Auger-electrons or, as in our case, the current from the sample, arising at the compensation of the electron emission from the sample.

The XANES spectra reflect the data on the distribution of the local partial density of free electron states in the conduction band. The $\mu(h\nu)$ is:

$$\mu(h\nu) \sim \nu^3 \Sigma_c |M_{ci}|^2 \delta(E_c - E_i - h\nu), \quad (1)$$

where $M_{ci} = \int \varphi_c H' \varphi_i dr$ is the matrix element of the transition probability of the electron from the core level with the wave function φ_i and eigenvalue E_i to the conduction band with the wave function φ_c and the eigenvalue E_c [13].

According to [12], for a given slip angle θ the quantum yield χ of electrons is proportional to the extinction coefficient μ, but also depends on the radiation reflection coefficient R:

$$\chi = \{[1 - R(\theta)]hc/4E\lambda\} \cdot (\mu/\sin\theta), \quad (2)$$

where E is average energy spent on the formation of electrons, λ is wavelength, h is Planck's constant, c is the speed of light.

In a common case, when the slip angle is substantially greater than the critical value for total external reflection, the value of the reflection coefficient $R(\theta)$ approaches zero, and the dependence of the quantum yield on the energy of the quant follows the spectral dependence of μ, that is used to measure XANES spectra of various objects in the ultrasoft field X-ray radiation. However, since the reflection coefficient $R(\theta)$ should depend on the slip angle, we have registered the XANES spectra of the studied porous-Si samples and the reference samples at different slip angles θ = 90°, 60°, 30°, and 10°. The measurements showed the absence of any difference in the recorded spectra for all values of θ, except 10°. Therefore, we present the results for the values of θ = 90° and 10°.

The study by the method of ultrasoft X-ray emission spectroscopy (USXES) were carried out on a ultrasoft X-ray spectrometer-monochromator RSM-500. The $L_{2,3}$-spectra of silicon were obtained. The depth of analysis was 20 and 60 nm. The changing depth of the analysis was achieved by changing in the kinetic energy of the excitation spectrum of electrons (from 1 to 3 keV). The working vacuum in the X-ray tube and the volume of the spectrometer was ~10^{-6} Torr.

According to [13], the USXES spectra allow to determine the local partial density of occupied electronic states in the valence band of the investigated material. The intensity of X-ray emission bands in the one-electron approximation is [13]:

$$I(h\nu) \sim \nu^3 \Sigma_v |M_{iv}|^2 \delta(E_i - E_v - h\nu), \quad (3)$$

where $M_{iv} = \int \varphi_i H' \varphi_v dr$ is the matrix element of the transition probability of an electron from the valence band with the wave function φ_v and eigenvalue E_v to a vacancy in the core level with the wave function φ_i, H' is perturbation operator, $h\nu$ is the energy emitted by X-ray photon.

The analysis of the phase composition was carried out using computer simulation of complex X-ray emission band obtained experimentally as a combination of the X-ray emission bands in the USXES spectra of reference materials [14]. The USXES spectra of the reference samples were obtained for the following objects: monocrystalline silicon c-Si, amorphous silicon a-Si, low-coordination silicon a-Si(lc) (this phase with the coordination number 2.5 to 3 was observed in amorphous silicon films [15]), and two types of silicon oxides: an intermediate silicon oxide SiO_x and silicon dioxide, SiO_2.

Note also that the advantage of the methods USXES and XANES is that they provide information on the local electron density of the emitting or

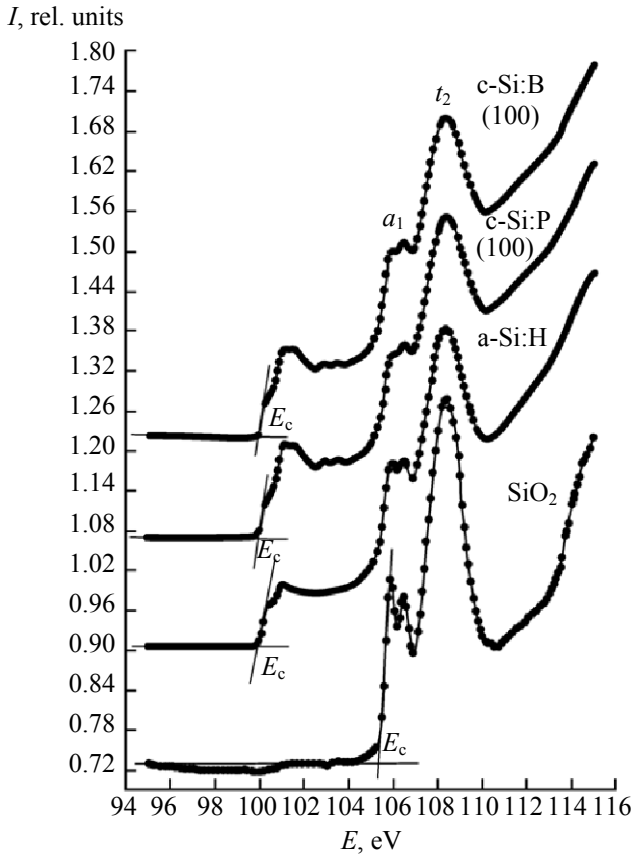

Fig. 1. XANES Si $L_{2,3}$ spectra of reference samples (θ = 90°).

absorbing atom. In addition, these methods are characterized by relatively high energy resolution and a simple interpretation of the results.

For all the samples were measured XANES spectra and USXES $L_{2,3}$ spectra of the silicon core level. The XANES spectra of all samples were measured in the region of the main $L_{2,3}$ extinction edges of elemental silicon and silicon oxide SiO_2 . Both of these edges are formed by electron transitions from the core levels $2p_{1/2,1/2}$ to the free states of the conduction band of Si and SiO_2. The binding energies for core levels of elemental silicon and silicon dioxide are 99.5 eV and 103.3 eV, respectively. Figure 1 shows the $L_{2,3}$ XANES spectra of the reference samples of monocrystalline phosphorus doped (c-Si:P) and boron doped (c-Si:B) silicon with a natural oxide layer on the surface of the both amorphous silicon (a-Si:H), and the film of thermal oxide SiO_2 30 nm thickness, which we used in the interpretation of XANES spectra of the porous silicon. The XANES spectra of c-Si (Fig. 1) consists of two main extinction edges: Si $L_{2,3}$ edge of the elementary c-Si (100 eV) and Si $L_{2,3}$ edge of the natural oxide (106 eV). The fine doublet structure of the main edges is due to the spin-orbit splitting of the core level Si $2p_{1/2,3/2}$ (0.6 eV), from which electrons are transferred to the conduction band of c-Si and SiO_2 at the excitation by the synchrotron radiation. The fine structure of the main edge (~100 eV) and next to it (~103 eV) is characteristic of single-crystal silicon, regardless of the orientation (100) or (111) and the type of conductivity, and disappears in the case of amorphous silicon a-Si:H, which shows one step only (~100.5 eV). The natural oxide layer on c-Si and a-Si:H, as well as thermal dioxide, keeps the structure of short-range order of silicon-oxygen tetrahedron T_d, which is reflected by the transitions from $2p_{1/2,3/2}$ level to the molecular orbitals σ*a_1 (Si 3*s*) and σ*t_2 (Si 3*p*). The close intensity of both $2p_{1/2,2/3} \rightarrow a_1$ (Si 3*s*) and $2p_{1/2,2/3} \rightarrow t_2$ (Si 3*p*) transitions is explainable by sp^3 hybridization of Si–O bonds in the tetrahedron.

It is known that the basic structural unit of thermally grown silicon dioxide is also the SiO_4 tetrahedron [16, 17]. The tetrahedra are connected via vertices by means of Si–O–Si bonds to form an irregular lattice. The main layer of high-quality thermal oxide grown in dry oxygen contains mainly the tetrahedra connected to form six-links rings, that is, the bond angle Si–O–Si is 144°. Between the layer of SiO_2 thermally grown on silicon and the silicon substrate there is a transition layer of dielectric with special structural properties, for which is characteristic the presence of strained Si–O bonds.

This layer consists of two areas: strained regions of thickness from 3 to 10 nm, in which an amorphous ring nets consist of three to four links with the Si–O–Si bond angles less than 144°, and the regions of thickness of the order of the monolayer with a variable chemical composition SiO_x [18]. However, as the depth of the investigation by XANES is ~5 nm, therefore because of the large thickness of the thermal oxide SiO_2 (> 30 nm), the composition of the transition layers SiO_2/c-Si has no effect on the fine structure of the XANES spectra.

Figures 2, 3, and 4 show the XANES Si $L_{2,3}$ spectra of porous-Si samples 0.5, 2.0, and 3.0. Already at a first glance these spectra show the difference of their main parameters from the parameters of the references. As these parameters were selected: I[L(Si)]/I[L(SiO_2)], the ratio of the intensities of the main extinction edges of Si $L_{2,3}$ of elementary (amorphous) silicon (101 eV) and of Si $L_{2,3}$ silica (106 eV), which characterizes the

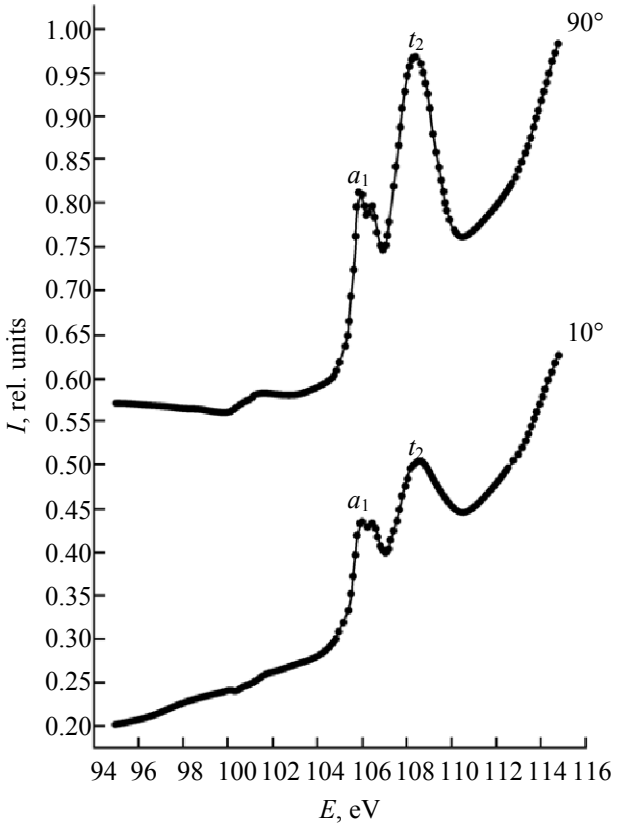

Fig. 2. XANES Si $L_{2,3}$ spectra of the sample of the porous silicon obtained at the etching duration 0.5 min, at different values of slip angle θ of synchrotron radiation.

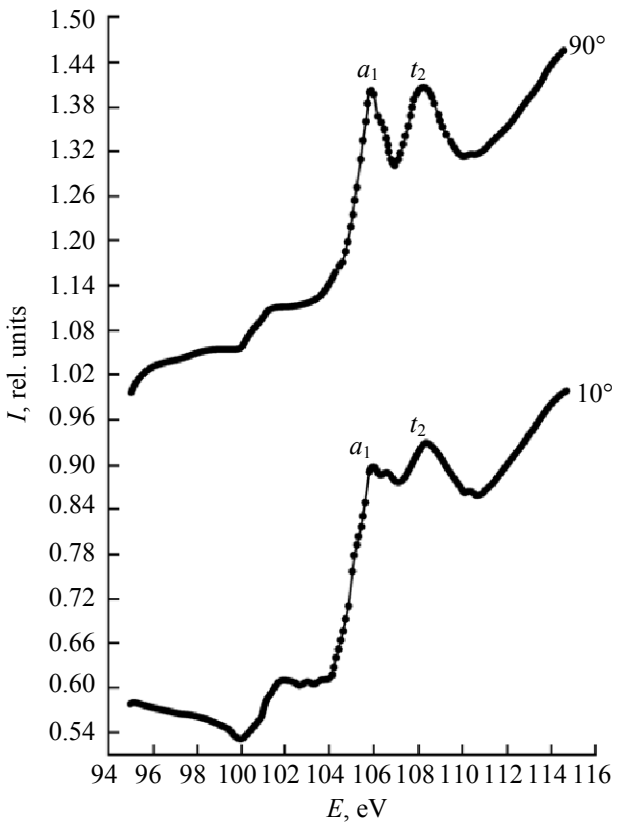

Fig. 3. XANES Si $L_{2,3}$ spectra of the sample of the porous silicon obtained at the etching duration 2 min, at different values of slip angle θ.

thickness of the oxide layer covering the layer of elemental (amorphous) silicon located beneath; Ia_1/It_2, the ratio of the intensities of the two main peaks in the XANES Si $L_{2,3}$ of the dioxide SiO_2, $Ia_1(3s)/It_2(3p)$, which characterizes the nature of the hybridization of the *s*, *p* states of σ* bonds in the silicon–oxygen tetrahedron; $\Delta E(t_2 - a_1)$, the energy difference between two peaks, $a_1(3s)$ and $t_2(3p)$, characterizing the presence or absence of deviation from the parameters of silicon–oxygen tetrahedron in α-quartz (bond lengths and bond angles), and the nature of packing of tetrahedra (average order).

The values of all these parameters of XANES Si $L_{2,3}$ spectra of three porous-Si samples and reference samples c-Si:P, c-Si:B, a-Si, and thermal SiO_2 are listed in Table 1. In addition, at the end of the list of samples, in Table 1 are shown the found by us certain values Ia_1/It_2 from the XANES Si $L_{2,3}$ spectra of crystalline SiO_2 of different modifications: α-quartz, crystobalite, stishovite, opal and coesite which were obtained by Dien Li et al. [19] at the same synchrotron SRC, that our spectra XANES. In Table 2 we present the data from the same publication of the parameters characterizing the silicon–oxygen tetrahedra of the crystallographic modifications of SiO_2 used below when discussing the results of research by the XANES method of the samples of porous silicon 0.5, 2.0, and 3.0.

Analysis of the intensity ratio of the major edges listed in Table 1 for the wafers of differently doped monocrystalline silicon shows that c-Si(100):R and c-Si(100):B wafers are covered with a natural SiO_2 layers of approximately equal thickness (~1 nm), while amorphous silicon is covered with a rather thick layer of oxide. At the same time, the a_1/t_2 ratio of peak intensities of the oxide itself shows that the structure of the silicon–oxygen tetrahedra of the a-Si:H surface oxide is close to the same of thermal oxide (both oxide show the value of Ia_1/It_2 close to 0.50). A lower value (~0.40) for the natural oxide monocrystal wafers reveals deviation from the stoichiometry of the oxide layer to the direction of the oxygen deficiency [20]. In

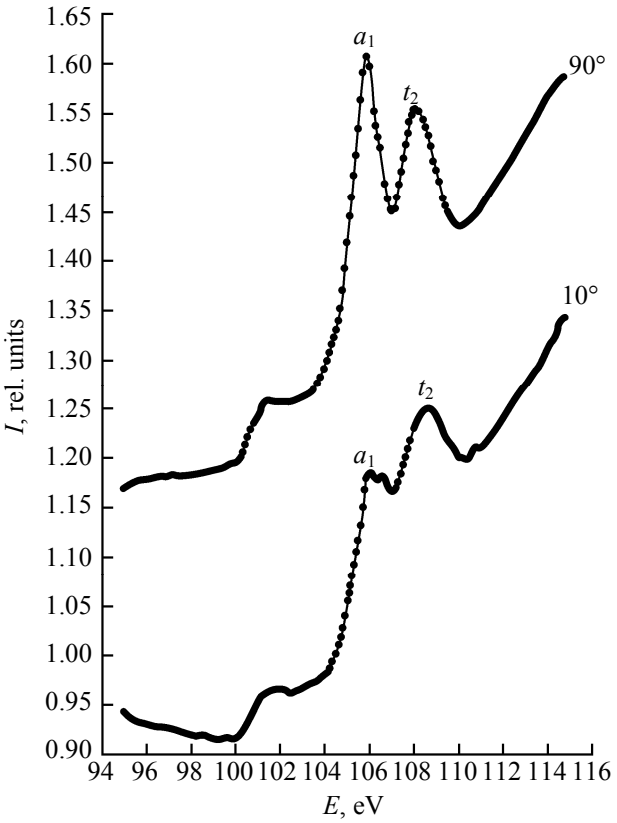

Fig. 4. XANES Si $L_{2,3}$ spectra of the sample of the porous silicon obtained at the etching duration 3 min, at different values of slip angle θ.

[19] were given the XANES Si $L_{2,3}$ spectra of SiO_x obtained by ion implantation of oxygen into c-Si(100) silicon, showing that with decreasing x from 1.8 to 0.4 the Ia_1/It_2 magnitude also falls from 0.66 to 0.59.

Analysis of the same parameters of the XANES Si $L_{2,3}$ spectra of porous-Si samples obtained at different duration of anodic etching shows, firstly, that oxide layer on the surface of the porous silicon of all the samples is much thicker than the natural oxide layers on c-Si and a-Si. The thickest layer is on the porous silicon (0.5), obtained at the least etching duration 0.5 min and least etching current density. But the most interesting is the fact that all the deviations of Ia_1/It_2, especially for the porous silicon (2) and porous silicon (3), exceed the corresponding values for the thermal SiO_2 (0.5), and even quartz (0.64) and approach the corresponding values in crystobalite (0.80) and coesite (0.90), and even higher than the values for the porous silicon (2) at all slip angles and for the porous silicon (3) at θ = 90°.

Analysis of the short-range parameters in three different modifications of SiO_2: α-quartz, α-crystobalite and coesite, in Table 2, led us to a conclusion that the increase in the ratio of intensities of peaks a_1/t_2 in this series was defined by a significant increase in the Si–O–Si bond angle and the distance between silicon atoms Si···Si, namely, by the distortion of the silicon–oxygen tetrahedra in going from α-quartz to coesite. While for the porous silicon oxide (0.5) the parameters of these tetrahedra vary between the parameters of α-quartz and α-crystobalite, the parameters of the porous silicon (2) exceed those of coesite. They reach the maximum deviation in the depth of the oxide layer of the porous silicon (3) with $a_1/t_2 = 1.18$, returning to the parameters of α-crystobalite on the surface of this layer, $a_1/t_2 = 0.78$ at θ = 10°.

The changes in the energy gap between the main peaks of σ orbitals $a_1(3s)$ and $t_2(3p)$, marked by us as $\Delta E(t_2 - a_1)$, point to the same distortion parameters of short-range order in the silicon – oxygen tetrahedron. In Table 3 these changes are given for the three porous-Si samples, reference samples, and various modifications of SiO_2. They vary from the maximum value of 2.6 eV in opal to a minimum of 1.9 eV in coesite. In the sample of porous silicon (0.5) the $\Delta E(t_2 - a_1)$ parameter is closest to the same parameter in the oxide a-Si:H (2.47), and only on the surface (θ = 10°) it becomes close to the same parameter of opal. In the sample of porous silicon (2) this value is lower (2.34 eV), and it reaches a minimum value in the

Table 1. Selected parameters of XANES Si $L_{2,3}$ spectra

Sample	I L(Si)/I L(SiO_2)		$I\,a_1/I\,t_2$	
	90°	10°	90°	10°
c-Si(111):P	1.70	1.70	0.34	0.37
c-Si(100):B	1.00	0.60	0.42	0.63
c-Si(100):P	1.00	1.20	0.39	0.45
a-Si:H	0.50	0.40	0.49	0.60
Porous silicon (0.5 min)	0.11	0.17	0.59	0.70
Porous silicon (2 min)	0.35	0.11	0.98	0.92
Porous silicon (3 min)	0.18	0.20	1.18	0.78
Thermal SiO_2			0.50	0.50
Opal [18]			0.44	
α-SiO_2 quartz [18]			0.64	
SiO_2 [15] crystobalite			0.80	
SiO_2 coesite [18]			0.90	

Table 2. The Si–O bond lengths and Si–O–Si bond angles of some crystalline forms of silica [18]

Parameter	α-quartz	α-crystobalite	coesite
Si:O (coordination number)	4:2	4:2	4:2
Si–O (Å)	1.61	1.605	1.61
Si–Si (Å)	3.06	3.07	3.09
Si–O–Si (deg)	144.0	146.8	150.8

porous silicon (3), $\Delta E(t_2 - a_1) = 2.25$ eV at $\theta = 90°$, while the ratio Ia_1/It_2 in its spectrum reaches maximum value. Thus, in the depth of the oxide layer of this sample, which is the boundary with an amorphous layer covering the nanocrystals porous silicon (3), occurs an increase of not only the Si–O bond length, but also increase of the Si–O–Si angles, which approach the values similar those in coesite (Tables 1–3).

Now, let us consider the data obtained by USXES. Figure 5 shows the Si $L_{2,3}$ USXES spectra of reference samples used for modeling and analysis. Note a change in the distribution of the local partial density of occupied states. In the case of amorphous silicon a complete blurring of the density of states and absence of features is seen that characterize disordered structure of the amorphous material [21]. In the case of low-coordination silicon a-Si(lc), the spectrum structure corresponds to the distribution of the density of states in c-Si (the position of individual peaks) in amorphous silicon (blurring of the spectrum). In the case of the silicon oxides, the distribution of the density of states is changed considerably compared to the crystalline and amorphous silicon due to the formation of SiO bonds and depending on the degree of oxidation differs by the relative intensity of peaks (Fig. 5).

Study of the samples of porous silicon by USXES confirms the conclusion about a significant distortion of the silicon–oxygen tetrahedron. Figure 6 shows the ultrasoft X-ray emission spectra of the samples. Comparison of the obtained emission spectra with the references shows that surface layers of porous silicon are much more amorphous. There are two peaks at energies 89 and 95 eV comparable by shape and position to those of the reference spectra of SiO_2 (and suboxide SiO_x) that indicates sufficient oxidation of the porous silicon layers. Nevertheless, the presence of spectral features in the region of ~92 eV indicates the presence in the samples of an ordered elemental silicon which follows from the comparison with the spectra of reference monocrystalline c-Si silicon.

Table 3. Energy gap (eV) between the two major molecular orbitals $a_1(3s)$ and $t_2(3p)$ in the samples of porous silicon, reference samples, and in some crystalline forms of silicon dioxide

Sample	$\Delta E(t_2 - a_1)$, eV	
	90°	10°
c-Si:P	2.42	
c-Si:B	2.42	
a-Si:H	2.47	
Porous silicon (0.5 min)	2.47	2.61
Porous silicon (2 min)	2.34	2.43
Porous silicon (3 min)	2.25	2.61
Thermal SiO_2	2.52	
Opal [18]	2.60	
α-SiO_2 quartz [18]	2.40	
SiO_2 [15] crystobalite	2.40	
SiO_2 coesite [18]	1.90	

The results of phase analysis are shown below.

Sample porous silicon (0.5) porous silicon (2) porous silicon (3)

Sample	Porous silicon (0.5)	Porous silicon (2)	Porous silicon (3)
c-Si, %	28.2	0	15.8
a-Si:H, %	22.6	2.3	36.5
a-Si(lc), %	0	29.7	0
SiO_2, %	0	67.9	42.6
$SiO_{1,3}$, %	49.2	0	5.2
Error, %	5.47	7.24	9.84

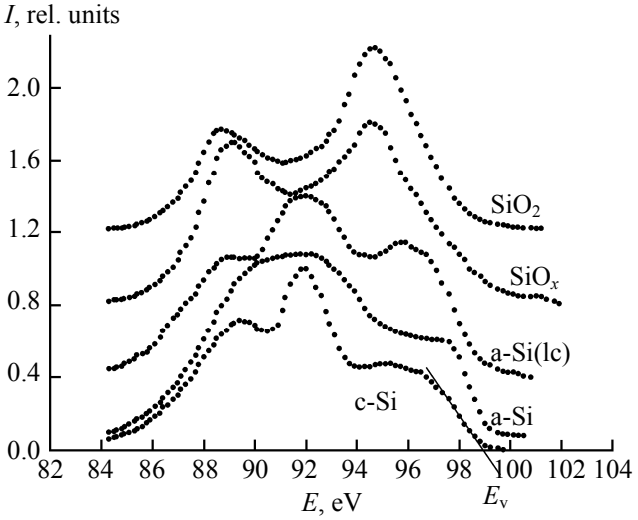

Fig. 5. USXES Si $L_{2,3}$ spectra of reference samples.

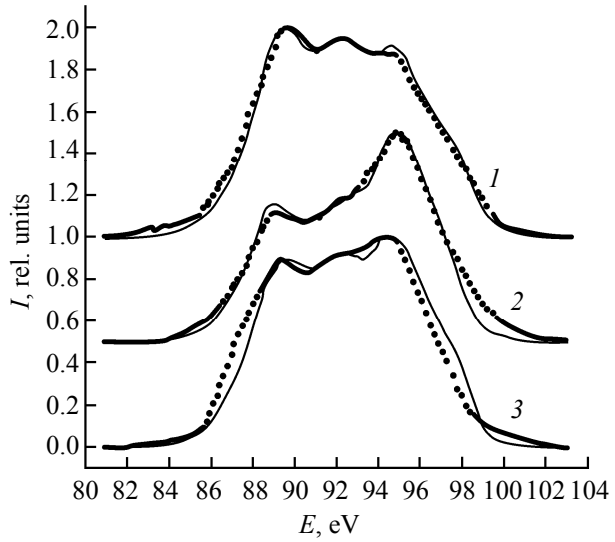

Fig. 6. USXES Si $L_{2,3}$ spectra of porous silicon obtained at different duration of etching: (*1*) porous silicon (0.5 min), (*2*) Porous silicon (2.0 min), and (*3*) porous silicon (3.0 min). The analysis depth is 60 nm.

Analysis of the phase composition of the surface layers of porous silicon on the basis of the obtained USXES spectra also shows a strong enough amorphization, together with the oxidation, revealing the presence of the intermediate suboxide SiO_x. Moreover, we found the presence of the ordered elemental Si in the investigated layers.

Note that the results obtained using the method USXES and the carried out phase analysis confirm the conclusions made previously in our papers [2–4, 10] that porous silicon is a complex multiphase formation consisting of crystalline silicon with different structural distortions (indicating the developed surface of porous silicon) which is oxidized, in particular, nonstoichiometrically.

Thus, using the spectral parameters of the XANES Si $L_{2,3}$ extinction of elemental silicon and silicon oxide we estimated the relative thickness of surface oxide nanolayers in porous silicon $I[L_{2,3}\ (Si)]/I[L_{2,3}\ (SiO_2)]$, and the nature of distortion of Si–O bonds in the silicon–oxygen tetrahedra of the layer, Ia_1/It_2 and $\Delta E(t_2 - a_1)$.

The thickness of the surface oxide layer in porous silicon after storage for one year becomes several times greater than the thickness of natural oxide silicon wafers of phosphorus and boron doped silicon with the orientation (100).

The data obtained by the XANES method show a significant distortion of the silicon–oxygen tetrahedron with elongation of Si–O bonds and increase in the Si–O–Si angles to a level comparable with the corresponding values in coesite.

The data obtained by the USXES method confirm the results obtained and show a fairly strong amorphization of the surface layers of the samples of porous silicon, together with their oxidation, revealing existence of the itermediate suboxide SiO_x. Moreover, we showed the presence of the ordered elemental Si in the investigated layers.

ACKNOWLEDGMENTS

This work was performed at the Synchrotron Radiation Center, University of Wisconsin–Madison, with support from NSF (grant no. DMR-0537588), and supported by the Federal target program “Research and scientific-pedagogical personnel of the Innovative Russia” for 2009–2013.

REFERENCES

1. Tolstoy, V.P., Chernyshova, I.V., and Skryshevsky, V.A., *Handbook of IR Spectroscopy of Ultrathin Films*, New Jersey: Wiley, 2003.
2. Domashevskaya, E.P., Kashkarov, V.M., Manukovskii, E.Yu., et. al., *J. Electr. Spectr. and Rel. Phen*., 1998, vols. 88–91, p. 969.
3. Domashevskaya, E.P., Terekhov, V.A., Kashkarov, V.M., et al, *FTT*, 2004, vol. 46, p. 335.
4. Turishchev, S.Yu., Lenshin, A.S., Domashevskaya, E.P. et al., *Physica Status Solidi, C*, 2009, vol. 6, no. 7, p. 1651.
5. Canham, L.T., *Appl. Phys. Lett*., 1990, vol. 57, p. 1046.
6. John, G.C. and Singh, V.A., *Phys. Rev. B*, 1994, vol. 50, p. 5329.
7. Yung, K.M., Shin, S., and Kwong, D.L., *J. Electrochem. Soc*., 1993, vol. 140, p. 3046.
8. Obraztsov, A.N., Timoshenko, V.Yu., Okushi, Kh., and Vatanabe, Kh., *Fiz. Tekh. Poluprovodnikov*, 1999, vol. 33, p. 322.
9. Xi-Mao Bao, Xiang He, Ting Gao, et. al., *Solid State Communications*, 1999, vol. 109, p. 169.
10. Turishchev, S.Yu., Terekhov, V.A., Kashkarov, V.M., et. al., *J. Electron Spectr. and Rel. Phen*., 2007, vols. 156–158, p. 445.
11. Blokhin, M.A, *Rentgenovskie luchi* (X-Rays), Moscow: Gos. Izd. Tekhniko-Teoreticheskoi Literatury, 1953.
12. Rumsh, M.A., Lukirskii, A.P., and Shchemelov, V.N., *Izv. Akad. Nauk SSSR, Ser. Fiz*., 1961, vol. 25, no. 8, p. 1060.

13. Zimkina, T.M. and Fomichev, V.A., *Ul'tramyagkaya rentgenovskaya spektroskopiya* (Ultra-Soft X-Ray Spectroscopy), Leningrad: Leningrad. Gos. Univ., 1971, p. 132.

14. Terekhov, V.A., Kashkarov, V.M., et. al., *J. Electron Spectr. and Rel. Phen*., 2001, vols. 114–116, p. 895.

15. Mashin, A.I., Khokhlov, A.F., Domashevskaya, E.P., Terekhov, V.A., and Mashin, N.I., *Fiz. Tekh. Poluprovodnikov*, 2001, vol. 35, p. 995.

16. Litovchenko, V.G. and Gorban', A.P., *Osnovy fiziki mikroelektronnykh sistem metall–dielektrik–poluprovodnik* (Fundamentals of the Physics of Micriolectronic Systems of Metal–Dielectric Semiconductor), Kiev: Naukova Dumka, 1978.

17. Nicollian, E.H., *MOS (Metal Oxide Semiconductirs) Physics and Technology*, New York: Wiley, 1984.

18. Grunthaner, F.J., Grunthaner, P.J., and Maserian, J., *IEEE Trans., Nuclear Physics*, 1982, vol. 29, no. 6, p. 1462.

19. Dien, Li, Bancroft, G.M., Kasrai, M., et. al., *American Mineralogist*, 1994, vol. 79, p. 622.

20. Baba, Y., Yamamoto, H., and Sasaki, T.A., *Phys. Rev., B*, 1993, vol. 48, no. 15, p. 10972.

21. Terekhov, V.A. and Domashevskaya, E.P., *Izv. Akad. Nauk SSSR, Ser. Fiz*., 1985, vol. 49, p. 1531.